Synthesis and Reactivities of Conducting Hexathienylbenzene-Co-Poly(3-Hexylthiophene) Star-Branched Copolymer as Donor Material for Organic Photovoltaic Cell

Morongwa E. Ramoroka[1]*, Siyabonga B. Mdluli[1], Vivian S. John-Denk[1], Kaylin C. Januarie[1], Kwena D. Modibane[2], Kelechi C. Nwambaekwe[1], Sodiq T. Yussuf[1], Kefilwe V. Mokwebo[1], Avril R. Williams[3] and Emmanuel I. Iwuoha[1]*

[1]SensorLab (Sensor Laboratories), University of the Western Cape, Bellville, South Africa, [2]Department of Chemistry, School of Physical and Mineral Sciences, University of Limpopo, Sovenga, South Africa, [3]Department of Biological and Chemical Sciences, The University of the West Indies, Cave Hill, Barbados

The hexathienylbenzene-co-poly(3-hexylthiophene-2,5diyl) (HTB-co-P3HT) conducting polymer was synthesized by oxidative co-polymerization of hexathienylbenzene (HTB) and 3-hexylthiophene using iron chloride ($FeCl_3$) as an oxidant. The effect of chlorobenzene, toluene and chloroform on the optoelectronic characteristics of the polymer was investigated. The study revealed that spectroscopic and electrochemical responses of HTB-co-P3HT are affected by the nature of the solvent. The lowest unoccupied molecular orbital (LUMO) and highest occupied molecular orbital (HOMO) energy levels of HTB-co-P3HT were determined from cyclic voltammetry (CV) and were compared to those of (6,6)-Phenyl C71 butyric acid methyl ester ($PC_{71}BM$) and it was found that the LUMO energy levels of HTB-co-P3HT in toluene were lower than those for chlorobenzene and chloroform. The electrochemical impedance spectroscopy (EIS) analysis also revealed the thin film of HTB-co-P3HT prepared using toluene as the most conductive. However, the photovoltaic parameters of the HTB-co-P3HT organic photovoltaic cells (OPVs) departed from the favored toluene and noted chlorobenzene as being the advantageous solvent. We obtained a power conversion efficiency (PCE) of 0.48%, fill factor (FF) of 27.84%, current density (J_{SC}) of 4.93 mA.cm^{-2} and open circuit voltage (V_{OC}) of 0.35 V in chlorobenzene, a PCE of 0.30%, FF of 26.08%, J_{SC} of 5.00 mA.cm^{-2} and V_{OC} of 0.23 V in chloroform and finally, a PCE of 0.33%, FF of 25.45%, J_{SC} of 5.70 mA.cm^{-2} and V_{OC} of 0.23 V in toluene.

Keywords: functional polymer, hexathienylbenzene-co-poly(3-hexylthiophene-2,5diyl), organic photovoltaic cells, oxidative co-polymerization, solar cell, solvent effect

1 INTRODUCTION

The high resistivity of organic polymers restricted their use to insulators in electrical applications prior to the discovery of conducting polymers (Le et al., 2017). Intensive research efforts bore polypyrrole as the first organic polymer displaying notable conductivity (Rasmussen, 2015; Chan et al., 2021) arising from alternating single and double bonds along the polymer chain (Bahceci and Esat, 2013; Khokhar et al., 2021). Today, this utilitarian conjugation has driven the development of many conducting polymers such polycarbazoles (Nayana and Kandasubramanian, 2020), polythiophenes (Valderrama-García et al., 2016), polyaniline (Boeva and Sergeyev, 2014) and polynaphthylamine (Pei et al., 2019). Further, conducting polymers have received recognition in such diverse research fields as organic light emitting diodes (Chen et al., 2020), organic field-effect transmitters (Afraj et al., 2021), supercapacitors (Wang et al., 2020), biosensors (Gupta et al., 2020) and OPVs (Liu et al., 2021), amongst others.

Conducting polymers have gained a lot of interest in the area of optoelectronics because of advantages such as low cost, tunability of optical properties, lightweight nature and flexibility (Dikcal et al., 2020). The properties of conjugated polymers can be tweaked either through modification of the side chains or the main chain (Zhou et al., 2012). Studies have shown that polymerization of monomeric fused rings tend to narrow the optical band gap, increase the conjugation length and expand the limits of light absorption (Gao et al., 2020; Tang et al., 2020; Xiao et al., 2020; Zhang et al., 2021; Zheng et al., 2021). Alkyl group substitution of either main chain or the side chain resulted in improved solubility of the polymer, reduced recombination rates and lower LUMO energy levels of the donor material ensuring efficient electron transfer activities to the acceptor component (Cui et al., 2011; Ye et al., 2013). Moreover, the introduction of electron-withdrawing groups into conjugated polymers was reported to modulate the molecular energy levels and aggregation morphologies leading to higher charge carrier mobility (Zhang et al., 2018).

Poly (3-hexylthiophene) (P3HT) is a conjugated polymer that is an attractive donor material candidate for use in OPVs owing to its facile synthesis and favourable charge transport properties. However, it has a wide band gap of ~1.9 eV which limits its photon absorption properties. The unrealized PCE of P3HT-based photovoltaic cells is mostly attributed to decreased open circuit voltages resulting from the high HOMO energy levels of P3HT (Cui and Wong, 2016). Many efforts have been targeted at the adjustment of the HOMO energy level to a more opportune position that can allow efficient charge transfer. In one such report, the hexyl group on the 3-position of the thiophene ring was replaced by an alkoxy group, which manifested in a raised HOMO energy level and improved photon absorption efficiencies by way of a reduced band gap, with concomitant decreased oxidation potential (Shi et al., 2006). Subsequent end-group modification of P3HT at the α-position of the last thiophene in the polymer chain with bromine accounted for a diminished overall performance of the device owing to trapped charges and more disordered morphological characteristics (Tanaka et al., 2017). Researchers also observed blue shifts associated with the presence of bromine on the P3HT (Kim et al., 2007).

P3HT has been incorporated into various types of co-polymers to enable well-structured polymeric materials. Through divergent polymerization methods such as chemical oxidation, radical and ring-opening, P3HT has been coupled to symmetrical propeller-shaped molecules to produce star copolymers (Park et al., 2013). The soluble, six-armed conjugated organic polymer, HTB, is one such candidate that exploits the electroconductivity and favourable optoelectronic properties of thiophenes and has the desired shape for a core platform for the preparation of conducting star copolymers. HTB together with other simple, small thiophene-based organic molecules, that are easy to procure or synthesized and are cost-effective, have been hailed as some of the most promising hole-transporting materials to optimize the power conversion efficiencies of solar cells (Cui et al., 2018).
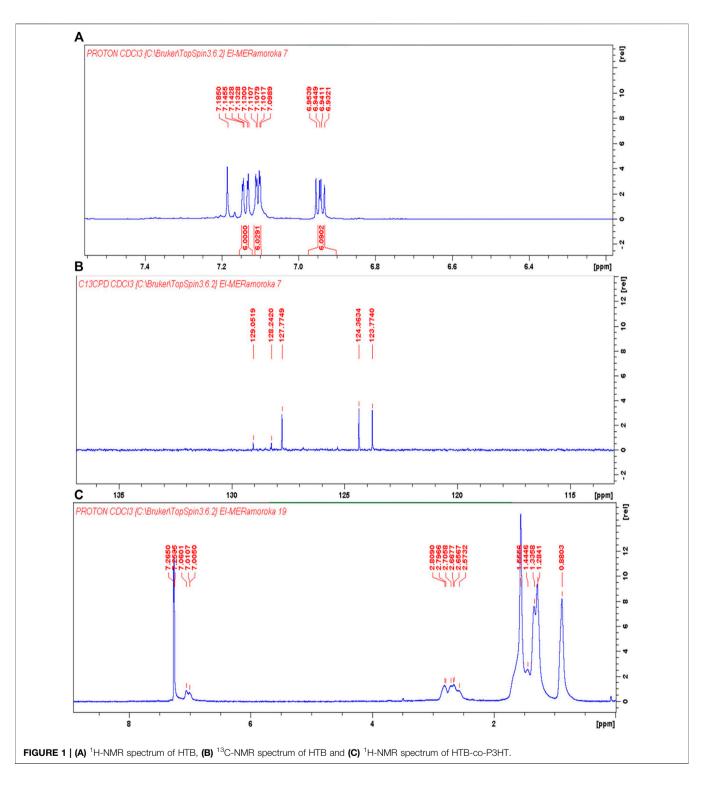
It has been shown that solvent nature, specifically polarity and volatility, affects the crystalline morphologies of polymeric thin films and hence the performance of devices targeted as OPVs. PCE and J_{SC} are two of the photovoltaic parameters of donor materials that showed improvement with increasing volatile solvent characteristics (Kim, 2019).

Herein, we report on a novel HTB-co-P3HT dendritic co-polymer, with HTB as a core, synthesized using CH-CH arylation method and Stille coupling reaction. The effect of P3HT on the surface of HTB and the energy levels of HTB-co-P3HT are studied in different solvents—chlorobenzene, toluene and chloroform—and compared to those of the highly efficient electron acceptor, PC$_{71}$BM. OPV devices of HTB-co-P3HT were also fabricated and it was revealed that the choice of solvent directly influences the photovoltaic parameters of HTB-co-P3HT as a donor material with chlorobenzene being the preferred solvent.
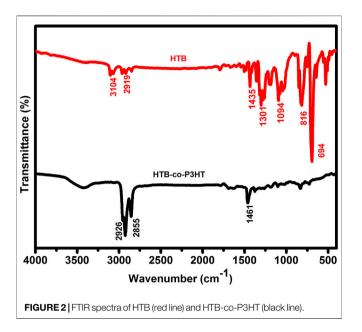
2 MATERIALS AND METHODS

2.1 General

Unless otherwise noted, all materials were used without further purification and were purchased from commercial sources. Deionized water was obtained from a Millipore Direct Q3 system (Millipore, Milford, MA, United States). ^{1}H and ^{13}C nuclear magnetic resonance (NMR) spectra were recorded on a Bruker 400 MHz Avance III HD Nanobay spectrometer. Proton chemical shifts are expressed in parts per million (ppm, δ scale) and are referenced to residual protium in deuterated chloroform (CDCl$_3$, δ = 7.26 ppm). Carbon chemical shifts are expressed in parts per million (ppm, δ scale) and are referenced to the carbon resonance of CDCl$_3$. Fourier transform infrared (FTIR) spectra were recorded on a Perkin-Elmer Spectrum-100 FTIR spectrophotometer. Thermal gravimetric analysis (TGA) measurements were obtained on a Perkin Elmer STA 6000 thermal analyser at a rate of 10°C/min under a N$_2$ flow rate of 20 ml/min. Room temperature ultraviolet-visible (UV-Vis) spectra were recorded on a Thermo Electron Corporation Nicolet Evolution 100. Transmission Electron Microscopy (TEM)

FIGURE 1 | (A) ^{1}H-NMR spectrum of HTB, **(B)** ^{13}C-NMR spectrum of HTB and **(C)** ^{1}H-NMR spectrum of HTB-co-P3HT.

images were obtained for the synthesized polymers using a FEI Tecnai T20 TEM while Scanning Electron Microscopy (SEM) images were acquired on a Tescan MIRA3 RISE SEM. Elemental composition data were collected on a FEI NovaNano SEM and photoluminescence spectral traces were obtained from a Horiba Jobin Yvon NanoLog. CV and EIS studies were conducted on a CHI700E-potentiostat where measurements were performed

using indium tin oxide (ITO) glass substrate (14–16 Ω/square resistance) as working electrode, platinum wire as counter electrode and silver/silver chloride (Ag/AgCl) as reference electrode in 0.1 M tetrabutylammonium hexafluorophosphate (TBAPF$_6$)/acetonitrile as electrolyte. The ITO glass substrate was washed with 1% (by volume) Hellmanex III solution, acetone and 2-propylalcohol prior to use. Device characteristics

FIGURE 2 | FTIR spectra of HTB (red line) and HTB-co-P3HT (black line).

FIGURE 3 | TGA thermogram of HTB-co-P3HT.

[current density–voltage (J-V)] were measured with an X200 Source Meter Unit from Sciencetech Inc. under an illumination of AM 1.5 G, with light intensity of 100 mW cm^{-2}.
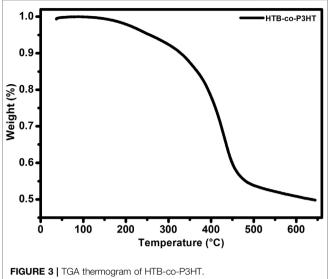
2.2 Synthesis
2.2.1 Synthesis of Hexathienylbenzene
One of the most popular methods for the synthesis of carbon-carbon bonds is the Stille coupling reaction (Zhang et al., 2015; Campos and Berteina-Raboin, 2020) which was utilized for the synthesis of HTB (**Scheme 1A**). Hexabromobenzene (0.50 g, 0.90 mmol), 2-(tributylstannyl)-thiophene (2.02 g, 0.54 mmol), copper(I) iodide (1.03 g, 0.54 mmol) and anhydrous potassium carbonate (0.75 g, 0.75 mmol) were dissolved in toluene (100 ml) and the reaction mixture was stirred for 30 min at room temperature. Palladium tetrakis(triphenylphosphine) (5% mol, 0.31 g, 0.27 mmol) was then added to the solution after which the mixture was stirred at 110°C for 120 h under inert atmosphere (nitrogen gas). The solvents were then removed under reduced pressure and the residue was re-dissolved in dichloromethane (DCM). The resulting solution was washed three times with deionized water. Anhydrous magnesium sulfate was added to the combined organic layers after which the mixture was filtered to remove the suspended magnesium sulphate (MgSO$_4$). The filtrate was concentrated by rotary evaporation and the residue was purified using column chromatography [DCM:petroleum ether (PE) = 1:2, v/v] with silica gel as the stationary phase. The resulting yellow powder (HTB; 0.33 g) was obtained in 64% yield. ^{1}H-NMR (400 MHz, CDCl$_3$): δ_H 7.14 (dd, 6H); 7.10 (dd, 6H); 6.95 (dd, 6H); ^{13}C-NMR (100 MHz, CDCl$_3$): δ_C 123.8, 124.4, 127.8, 128.2, 129.1. FTIR (cm^{-1}): 3,104, 2,919, 1,435, 1,301, 1,094, 816, 694. UV-Vis (toluene, nm): 299, 385.
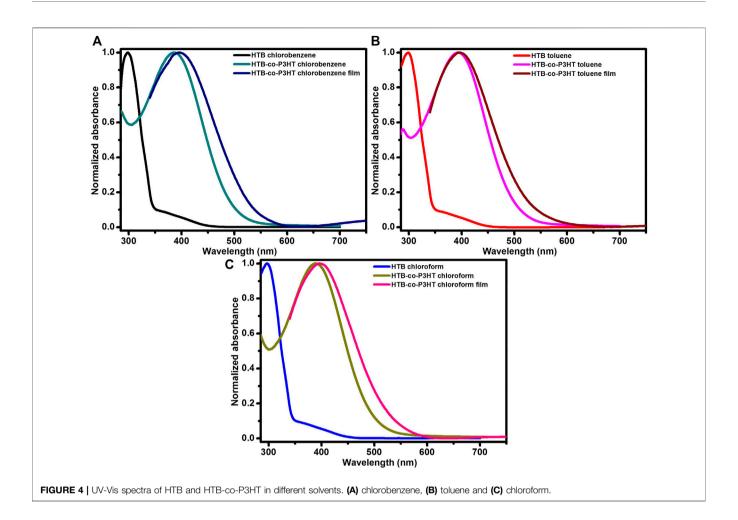
2.2.2 Synthesis of Hexathienylbenzene-co-P3HT
HTB-co-P3HT was synthesized (**Scheme 1B**) using CH-CH arylation method (Ansari et al., 2018; Ramoroka et al., 2021).

HTB (0.15 g, 0.26 mmol) and 3-hexylthiophene (1.42 ml, 1.33 g, 7.89 mmol) were added to chloroform (80 ml). The solution was stirred under nitrogen gas for 30 min, followed by the addition of anhydrous FeCl$_3$ (5.12 g, 0.03 mol) to form a suspension. The mixture was then refluxed for 24 h under inert atmosphere (N$_2$). Polymerization was then terminated by addition of anhydrous methanol (MeOH) and the precipitate was filtered and washed with Soxhlet extraction using acetone for 24 h followed by MeOH for a further 24 h. Subsequently, HTB-co-P3HT was extracted with DCM for 24 h resulting in a dark purple solid (0.28 g). ^{1}H-NMR (400 MHz, CDCl$_3$): δ_H 7.01 (m); 2.57–2.80 (m); 1.28–1.56 (m). FTIR (cm^{-1}): 2,926, 2,855, 1,461. UV-Vis (, nm): 393.

2.3 Organic Photovoltaic Cells Fabrication
OPVs fabrication and measurements were done under normal conditions. ITO glass substrates, after washing, were spin-coated with zinc oxide (ZnO) and annealed for 30 min at 100°C. ZnO was prepared using sol-gel method (Ramoroka et al., 2021). In details, ZnO solution was prepared using zinc acetate dihydrate as a precursor, 2-methoxyethanol as a solvent and monoethanolamine as a stabilizing agent. The precursor solution with a concentration of 0.5 M in methoxyethanol was prepared and was used to prepare 0.5 M monoethanolamine solution. The resulting solution was stirred at 60°C for 2 h and after aged for 24 h. The deposition was carried out using spin coating method. ZnO solution was spin coated at 3000 rpm for 60 s and dried at 100°C. The coating processes was repeated two times to increase the thickness of ZnO. After coating, ZnO films were annealed at 300°C for 1 h. The active layer was prepared by dissolving HTB-co-P3HT and PC$_{71}$BM in chlorobenzene for a total concentration of 25 mg/ml and the solution was stirred overnight at 60°C. The active layer was then spin-coated onto the ZnO/ITO glass substrate and annealed at 100°C for 5 min. Subsequently, a poly(3,4-ethylenedioxythiophene) polystyrene sulfonate (PEDOT:PSS) layer (0.5–1.0 wt.% in water) was spin-

FIGURE 4 | UV-Vis spectra of HTB and HTB-co-P3HT in different solvents. **(A)** chlorobenzene, **(B)** toluene and **(C)** chloroform.

coated and annealed at 150°C for 5 min. Finally, silver conductive paste was used to coat the cathode with drying at 100°C for 5 min to complete the OPVs. The active areas of OPVs are 0.0256 cm^2.

3 RESULTS AND DISCUSSION

3.1 Nuclear Magnetic Resonance Studies of Hexathienylbenzene and Hexathienylbenzene-Co-P3HT

The structure of HTB was confirmed by NMR spectroscopy. **Figures 1A,B** show the ^{1}H-NMR and ^{13}C-NMR spectra of HTB, respectively. The integrals on the ^{1}H-NMR spectrum indicate that a total of 18 protons were detected which corresponds to the number of protons on the HTB structure. The signals at 6.94 ppm and 7.14 ppm correspond to protons at the 4- and 3-positions of the thiophene moiety while the α-position is represented at 7.10 ppm. The ^{13}C-NMR spectrum of HTB showed the expected five signals at different chemical shifts. Both the ^{1}H and ^{13}C chemical shifts are in agreement with that reported in the literature (Leitner et al., 2020; Yoshida et al., 2008a; Yoshida et al., 2008b). The ^{1}H-NMR spectrum of HTB-co-P3HT (**Figure 1C**) is very different in appearance from that

of HTB. The signal at 0.88 ppm is assigned to the CH$_3$- of the hexyl group, the multiplets at 1.28–1.56 ppm and 2.57–2.80 ppm are attributed to the methylene protons from the hexyl group while the thiophene groups are signaled at 7.01 ppm (Mota et al., 2021; Yadav et al., 2021).
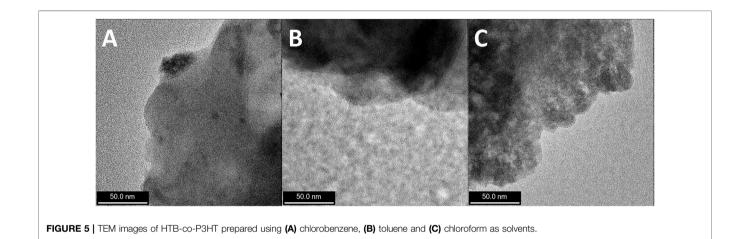
3.2 Fourier Transform Infrared Analysis of Hexathienylbenzene and Hexathienylbenzene-Co-P3HT

The synthesized HTB and HTB-co-P3HT were characterized by FTIR (**Figure 2**). The bands at 3,104 and 2,919 cm^{-1} in the spectrum of HTB are attributed to C–H stretching while the band at 816 cm^{-1} is ascribed to the in-plane bending vibration of the aromatic ring. The band at 1,094 cm^{-1} results from C–S vibrations. Additionally, the band at 694 cm^{-1} is due to the in-plane bend of the C–S–C of thiophene. The remaining bands at 1,435 and 1,301 cm^{-1} are assigned to the C = C and C–C of the thiophene ring, respectively (Agrawal et al., 2013). After formation of HTB-co-P3HT, strong bands at 2,926 and 2,855 cm^{-1} appear owing to the vibration of the C–H bond of the hexyl group (Tamanai et al., 2013). The C = C stretching vibration shifts to 1,461 cm^{-1} (from 1,435 cm^{-1}) subsequent to

TABLE 1 | UV-Vis responses of HTB and HTB-co-P3HT in various solvents.

Compound	Solvent	Maximum wavelength (nm)	Onset wavelength (nm)	Optical[a] band gap (eV)	Onset wavelength film (nm)	Optical band[a] gap film (eV)
HTB	Chlorobenzene	298	349	3.55	—	—
HTB	Toluene	299	350	3.54	—	—
HTB	Chloroform	296	348	3.56	—	—
HTB-co-P3HT	Chlorobenzene	386	520	2.38	578	2.15
HTB-co-P3HT	Toluene	393	530	2.34	589	2.12
HTB-co-P3HT	Chloroform	389	525	2.36	583	2.13

[a]Optical band gap = $1240/\lambda_{onset}$, where λ_{onset} is the onset wavelength.
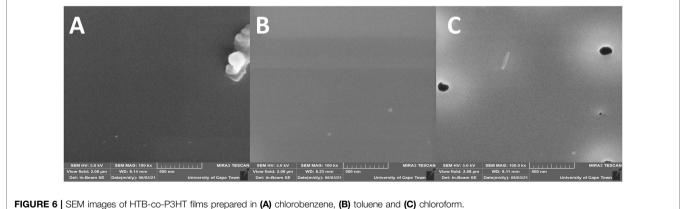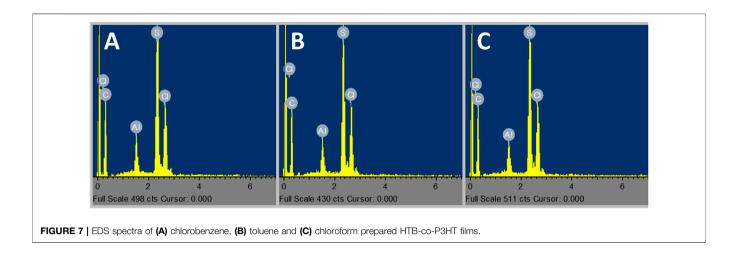

FIGURE 5 | TEM images of HTB-co-P3HT prepared using **(A)** chlorobenzene, **(B)** toluene and **(C)** chloroform as solvents.

FIGURE 6 | SEM images of HTB-co-P3HT films prepared in **(A)** chlorobenzene, **(B)** toluene and **(C)** chloroform.

the attachment of P3HT at the α-position of thiophene (Naureen et al., 2021) and indicates the successful attachment of P3HT on HTB.

3.3 Thermal Gravimetric Analysis Studies of Hexathienylbenzene-co-P3HT

Figure 3 shows a TGA thermogram of HTB-co-P3HT obtained from the co-polymerization of HTB and 3HT. The decomposition of HTB-co-P3HT takes place in three stages.

No weight loss was observed at a temperature range between 50°C and 130°C indicating the absence of adsorbed water on the surface of the sample (Joseyphus and Nair, 2010). In the second stage, weight loss of approximately 8% occurred in the 138°C–312°C temperature range and could be attributed to the decomposition of small molecular weight HTB-co-P3HT and newly formed HTB. Weight loss of 25% in the third stage (temperature range of 379°C–455°C) was observed and represents the decomposition of HTB-co-P3HT. Onset and maximum degradation temperature were found to be 150°C

FIGURE 7 | EDS spectra of **(A)** chlorobenzene, **(B)** toluene and **(C)** chloroform prepared HTB-co-P3HT films.

and 460°C, respectively. The remaining weight can be rationalized as solid residues (Khalaji and Das, 2015; Warad et al., 2020).

3.4 Ultraviolet-Visible Studies of Hexathienylbenzene and Hexathienylbenzene-co-P3HT in Different Solvents

The UV-Vis spectra of HTB and HTB-co-P3HT were recorded in different solvents at room temperature as depicted in **Figure 4**. One band was observed in the absorption spectra of HTB-co-P3HT while two bands appeared for HTB. The first band in the spectrum of HTB was assigned to the π→π* transitions and the second band results from the n→π* transitions (Leitner et al., 2020; Ramoroka et al., 2021). The conjugated P3HT chains on the surface of HTB are responsible for the single band in the spectrum of HTB-co-P3HT (Fei et al., 2015; Ramoroka et al., 2021). The absorption responses of the two compounds are collected in **Table 1**. The parameter dissimilarities are a consequence of the polarity differences of the solvents. The maximum wavelength and lowest band gap values were obtained in toluene. Because toluene stabilizes excited state by interacting with it resulting to a shift to longer wavelength (Sancho et al., 2011). Optical band gaps for HTB were determined to be 3.55, 3.54 and 3.56 eV, while for HTB-co-P3HT they were quantified as 2.38, 2.34 and 2.36 eV in chlorobenzene, toluene and chloroform, respectively. Optical band gaps of 2.15, 2.12 and 2.13 eV for thin films of HTB-co-P3HT prepared in chlorobenzene, toluene and chloroform, respectively were also recorded. These results indicate a bathochromic shift when chlorine atoms are absent on the solvent molecules. Since J_{SC} is inversely proportional to optical band gap, the highest J_{SC} can be achieved in toluene (Jeong et al., 2021) and heightened generation of electron-hole pairs in HTB-co-P3HT will preferentially also occur in toluene (Fan et al., 2021).

3.5 Transmission Electron Microscopy Studies of Hexathienylbenzene-co-P3HT

The morphologies of HTB-co-P3HT in different solvents were characterized using TEM (**Figure 5**). The HTP-co-P3HT particles are indicated by the high-contrast dark regions. It

was expected that chloroform, with its low boiling point and lowest surface tension (Birnie, 2013; Zhao et al., 2015), would show the most agglomeration as the HTB-co-P3HT particles would not have enough time to settle (fast evaporation) and would therefore lead to high reabsorption rates and decreasing V_{OC} (Liu et al., 2020). However, the same effect was observed for the co-polymer in toluene and to a lesser extent in chlorobenzene. Consequently, it is difficult to observe the effect of solvent on the morphology of HTB-co-P3HT owing to the similar agglomeration of the polymer particles.

3.6 Scanning Electron Microscopy Studies of Hexathienylbenzene-co-P3HT

Figure 6 shows the SEM images of HTB-co-P3HT films prepared in chlorobenzene (A), toluene (B) and chloroform (C) by drop coating onto ITO coated glass substrates. The SEM images revealed that the surface of HTB-co-P3HT is smooth, and that the morphology changes trend the changes in solvent. In one instance (chlorobenzene) there was some agglomeration of HTB-co-P3HT particles while in another (chloroform and toluene), no agglomeration was observed. The EDS spectra of HTB-co-P3HT (**Figure 7**) revealed the presence of carbon (C) and sulfur (S), arising from the synthesized HTB-co-P3HT polymer with little differentiation associated with the change in solvents. What was deemed to be an impurity chlorine (Cl) can be attributed to the oxidant, $FeCl_3$, employed during the polymerization process.

3.7 Photoluminescence of Hexathienylbenzene and Hexathienylbenzene-co-P3HT

Photoluminescence studies of HTB and HTB-co-P3HT in different solvents (**Figure 8**) present excitation spectra that are blue-shifted compared with the analogous emission spectra, suggestive of the loss of energy by the photogenerated excitons *via* either non-radiative or radiative processes before recombination (Chang et al., 2013). The emission spectra of HTB exhibited peaks at 365, 364 and 366 nm while excitation
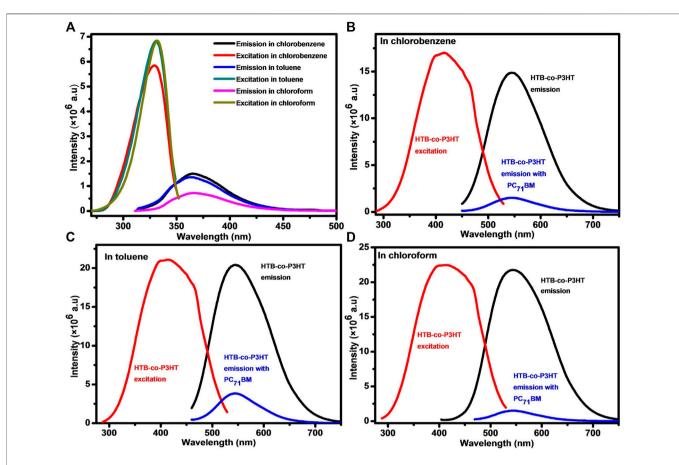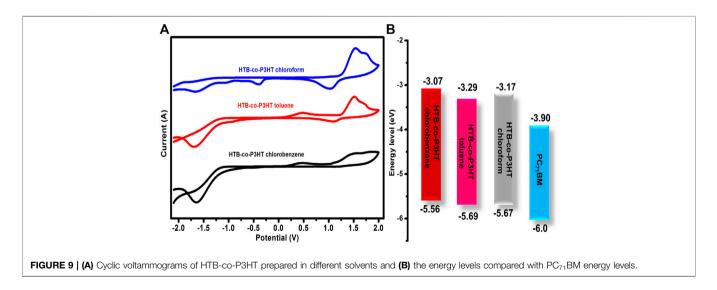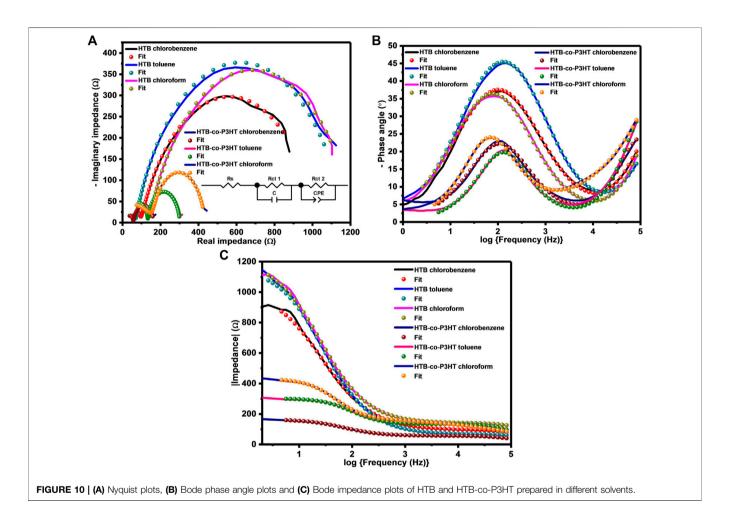
FIGURE 8 | (A) Photoluminescence spectra of HTB in different solvents. Photoluminescence spectra of HTB-co-P3HT in **(B)** chlorobenzene, **(C)** toluene and **(D)** chloroform.

FIGURE 9 | (A) Cyclic voltammograms of HTB-co-P3HT prepared in different solvents and **(B)** the energy levels compared with $PC_{71}BM$ energy levels.

spectra of HTB exhibited peaks at 329, 331 and 331 nm resulting in Stokes shifts of 36, 33 and 35 nm in chlorobenzene, toluene and chloroform, respectively. Larger Stokes shift for HTB-co-P3HT were determined to be 130, 133 and 131 nm in chlorobenzene,

toluene and chloroform, respectively, which can result from efficient energy transfer to lower energy levels and planarity enhancement of the P3HT polymer chain in HTB-co-P3HT (Hu et al., 2015). Meanwhile, in both cases, the relatively non-

TABLE 2 | Electrochemical properties of HTB-co-P3HT in different solvents.

Compound	E_{HOMO} (eV)	E_{LUMO} (eV)	ΔE_{LUMO} (eV)	$E_g{}^{CV}$ (eV)
$PC_{71}BM$	−6.0	−3.90	—	—
HTB-co-P3HT (chlorobenzene)	−5.56	−3.07	−0.83	2.49
HTB-co-P3HT (toluene)	−5.69	−3.29	−0.61	2.40
HTB-co-P3HT (chloroform)	−5.67	−3.17	−0.73	2.50

FIGURE 10 | (A) Nyquist plots, **(B)** Bode phase angle plots and **(C)** Bode impedance plots of HTB and HTB-co-P3HT prepared in different solvents.

polar toluene recorded the smallest Stokes shift values as expected (Hu et al., 2015). The intense emission peaks of HTB-co-P3HT suggest high recombination of holes and electrons (Liu et al., 2019). There being little difference between the band positions at 545 nm in chlorobenzene, 546 nm in toluene and 543 nm in chloroform indicates weak solvatochromism and suggests that the ground state energy levels of HTB-co-P3HT are independent of the solvent polarity (Ekbote et al., 2017).

Photoexcited charge transfer in the heterojunction between HTB-co-P3HT and $PC_{71}BM$ was investigated using photoluminescence. Emission spectra of HTB-co-P3HT and $PC_{71}BM$ blends are shown in **Figure 8**. The photoluminescence intensity of HTB-co-P3HT:$PC_{71}BM$ is lower than that of HTB-co-P3HT, indicating an increase in charge dissociation of photoexcited excitons and reduction of recombination activities in the former. The re-emergence of photoluminescence intensity of HTB-co-P3HT, quenched after blending with $PC_{71}BM$, are 89, 80 and 93% in chlorobenzene, toluene and chloroform, respectively. These results indicate that the greatest charge separation takes place in chloroform, the most polar of the solvents.

3.8 Cyclic Voltammetry Studies of Hexathienylbenzene-co-P3HT

The effect of solvent used in the preparation of the HTB-co-P3HT thin films was studied using CV. **Figure 9A** shows the cyclic voltammograms of HTB-co-P3HT thin films prepared using chloroform, toluene and chlorobenzene. The HOMO and LUMO energy levels were determined and compared with the
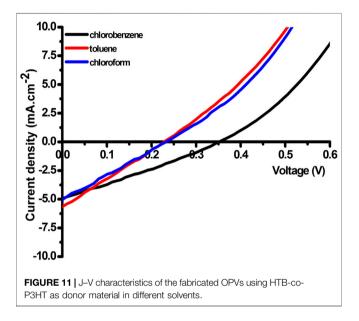
TABLE 3 | EIS results for HTB and HTB-co-P3HT prepared in various solvents.

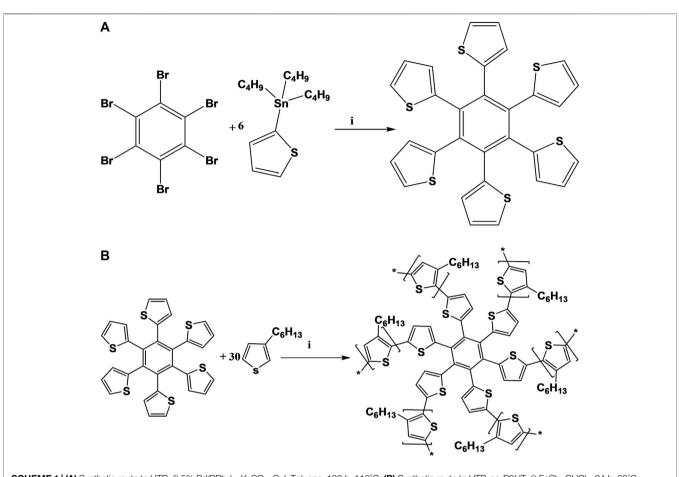| Compounds	R_s (Ω)	R_{ct} (Ω)	CPE-T	CPE-P	τ (ms)
HTB (chlorobenzene)	41.16 ± 1.95	939.70 ± 7.41	$3.44 \times 10^{-5} \pm 6.78 \times 10^{-7}$	$0.72 \pm 2.95 \times 10^{-3}$	1.52
HTB (toluene)	31.55 ± 1.57	1,109.0 ± 4.33	$2.31 \times 10^{-5} \pm 2.4 \times 10^{-7}$	$0.76 \pm 1.54 \times 10^{-3}$	1.13
HTB (chloroform)	43.46 ± 3.16	1,090.0 ± 3.89	$2.75 \times 10^{-5} \pm 2.82 \times 10^{-7}$	$0.74 \pm 1.60 \times 10^{-3}$	1.91
HTB-co-P3HT (chlorobenzene)	23.96 ± 0.52	109.70 ± 0.89	$7.88 \times 10^{-5} \pm 2.91 \times 10^{-6}$	$0.81 \pm 5.70 \times 10^{-3}$	1.52
HTB-co-P3HT (toluene)	40.56 ± 1.36	170.50 ± 1.24	$2.13 \times 10^{-5} \pm 8.50 \times 10^{-7}$	$0.90 \pm 6.10 \times 10^{-3}$	1.29
HTB-co-P3HT (chloroform)	54.89 ± 2.29	327.80 ± 10.543	$5.18 \times 10^{-5} \pm 6.25 \times 10^{-6}$	$0.75 \pm 19.3 \times 10^{-3}$	2.30

energy levels of P3HT and $PC_{71}BM$ and the data are collected in **Table 2**. The difference in the HOMO and LUMO energy levels (E_g^{CV}) of HTB-co-P3HT in toluene are less than those in the chlorinated solvents and results in a narrow electrochemical band gap. These observations can be attributed to the polarity and the boiling point characteristics of the solvents as increased polarity and decreased boiling points tend to result in augmented aggregation and energy band gaps (Niefind et al., 2019; Salaiman et al., 2019). The differences in polarity of the chloroform, toluene and chlorobenzene solvents might influence their interaction with the aromatic backbone and/or side groups of the polymer chain materialising as varying degrees of aggregation (Rahman et al., 2009; El-Bashir, 2019). This agglomeration factor may have contributed to the higher LUMO energy levels and wider electrochemical band gaps in chloroform and chlorobenzene. Further, the LUMO energy levels of HTB-co-P3HT in toluene, chloroform and chlorobenzene are −0.61, −0.73 and −0.83 eV above the LUMO energy levels of $PC_{71}BM$, respectively. These LUMO offset (ΔE_{LUMO}) values are significantly smaller in toluene than in chlorobenzene and chloroform which indicates that charge transfer from the LUMO of HTB-co-P3HT in toluene can occur more efficiently than if chlorobenzene and chloroform were used. However, high energy loss will still occur thereby lowering V_{OC} as ΔE_{LUMO} values are much higher than the threshold value of 0.3 eV (Gautam et al., 2017).

3.9 Electrochemical Impedance Spectroscopy Studies of Hexathienylbenzene and Hexathienylbenzene-co-P3HT

Electrochemical impedance spectra obtained for HTB and HTB-co-P3HT in different solvents are depicted in **Figure 10**. Nyquist plots were used to study charge carrier migration in the electrochemical cells. It is well-known that the charge transfer resistance (R_{ct}) is related to the diameter of the semicircle at the interface of an electrode and sample and that the smaller the diameter of the semicircle, the faster the diffusion of charges through the sample to the electroactive surface of the electrode. The Nyquist plot (**Figure 10A**) showed two semicircles, where the one at higher frequency corresponds to the resistance of the electrode whereas the other identifies with the ionic diffusion resistance of the electrolyte, charge transfer resistance or the resistance of the sample/electrolyte interphase layer (Mei et al., 2018). Both semicircles from the Nyquist spectra were fitted and

FIGURE 11 | J–V characteristics of the fabricated OPVs using HTB-co-P3HT as donor material in different solvents.

the results for the lower frequency trace are collected in **Table 3**. This study revealed that HTB and HTB-co-P3HT each display different electrochemical behaviour depending on the solvent. The smallest R_{ct} of 939.70 and 109.70 Ω were obtained for HTB and HTB-co-P3HT in chlorobenzene, respectively. This result indicates that the most efficient electron-hole pair separation and the fastest electron transfer at the sample/electrode interface occurs in chlorobenzene (Huang et al., 2013). The very noticeable reduction in the R_{ct} of HTB-co-P3HT when compared to HTB in chlorobenzene reveals the increased electron transfer between the electrode and electrolyte as a result of the presence of P3HT chains on the surface of HTB. It is noteworthy that the frequency of the maximum peak shifts to the left after modification of HTB with P3HT in both toluene and chloroform but remains unshifted in chlorobenzene (**Figure 10B**). The frequency shifts in chloroform and toluene indicate reduction of the recombination rate (Pei et al., 2016). Estimations of the electron lifetimes for HTB and HTB-co-P3HT revealed the highest values of 1.91 and 2.30 ms in chloroform. Conclusively, the most reduced rate of recombination and longer electron lifetimes were obtained in chloroform. **Figure 10C** shows the impedance vs frequency plot of HTB and HTB-co-P3HT prepared in different solvents. It was observed that HTB-co-P3HT has subjacent impedance at lower frequencies than HTB denoting faster electron conduction in HTB-co-P3HT, an

SCHEME 1 | (A) Synthetic route to HTB. (i) 5% Pd(PPh$_3$)$_4$, K$_2$CO$_3$, CuI, Toluene, 120 h, 110°C; **(B)** Synthetic route to HTB-co-P3HT. (i) FeCl$_3$, CHCl$_3$, 24 h, 60°C.

TABLE 4 | Photovoltaic performance of HTB-co-P3HT as donor material.

Donor material and solvent	PCE (%)	FF (%)	J$_{SC}$ (mA.cm^{-2})	V$_{OC}$ (V)	R$_S$ Ω.cm^2	R$_{Sh}$ Ω.cm^2
HTB-co-P3HT (chlorobenzene)	0.48	27.84	4.93	0.35	49.06	79.32
HTB-co-P3HT (toluene)	0.33	25.45	5.70	0.23	44.38	42.20
HTB-co-P3HT (chloroform)	0.30	26.08	5.00	0.23	43.97	52.12

$R_{Sh} = \frac{\Delta V}{\Delta I}, V = 0$ and $R_S = \frac{\Delta V}{\Delta I}, V = V_{OC}$.

observation consistent with the lower R$_{ct}$ obtained for HTB-co-P3HT.

3.10 Photovoltaic Properties of Hexathienylbenzene-co-P3HT

Figure 11 shows the current density-voltage (J-V) curves of HTB-co-P3HT, as a donor material, in different solvents and the key photovoltaic parameters for OPVs fabricated in ambient atmosphere are presented in **Table 4**. The maximum PCE was obtained in chlorobenzene, followed by toluene, then chloroform. This winning performance in chlorobenzene is due to fast electron transfer as confirmed by the prior detailed

EIS studies. However, the small FF and V$_{OC}$ values were realized for chloroform and toluene-prepared HTB-co-P3HT signifying the highest hole and electron charge recombination. This is supported by the higher R$_{ct}$ values obtained from EIS. Photoluminescence revealed that sufficient charges are separated at the interface of HTB-co-P3HT and PC$_{71}$BM film prepared in chloroform. But they turn to recombine because of poor conductivity of chloroform-prepared HTB-co-P3HT:PC$_{71}$BM film and agglomeration of HTB-co-P3HT observed on TEM images resulting in lower V$_{OC}$ and PCE. As all OPVs were fabricated using silver paste as the top electrode and in the ambient air, some degree of degradation may have occurred. The

architecture of the OPVs fabricated in this study was as follows: glass|ITO|ZnO|HTB-co-P3HT:PC$_{71}$BM|PEDOT: PSS|Ag paste. It has been revealed that spin-coating PEDOT:PSS results in the presence of pinholes (Ramoroka et al., 2021) and that direct contact between Ag paste and HTB-co-P3HT:PC$_{71}$BM led to diffusion of Ag paste into HTB-co-P3HT:PC$_{71}$BM active layer resulting in an increase in charge recombination (Kim et al., 2015). In addition, since our devices were fabricated in air, oxidized sulfur species may have formed in the active layer (Kettle et al., 2016) and consequently may act as charge carrier trapping sites (Rafique et al., 2020). Series resistance (R$_S$) and shunt resistance (R$_{Sh}$) were determined from the inverse of slopes near V$_{OC}$ and J$_{SC}$, respectively (Gholizadeh, et al., 2017; Diantoro et al., 2018). The R$_S$ and R$_{Sh}$ values are given in **Table 4**. High values of R$_S$ estimated lead to a decrease in I$_{SC}$ and maximum voltage, while low values of R$_{Sh}$ lead to a decrease in V$_{OC}$ and maximum current. Therefore, R$_S$ and R$_{Sh}$ are responsible for reduction of the FF (Wang et al., 2012).

4 CONCLUSION

In this report, HTB and HTB-co-P3HT were successfully synthesized using Stille coupling reaction and chemical oxidation polymerization, respectively. The structural characteristics of HTB were confirmed by ^{1}H and ^{13}C NMR spectrometry. FTIR corroborated the successful decoration of HTB by P3HT in the form of new bands at 2,926 and 2,855 cm^{-1} and a shift in wavenumber for the C = C vibration post-polymerization. The UV-Vis studies were performed in different solvents (chlorobenzene, toluene and chloroform) and the narrowest band gaps were achieved in toluene. CV interrogations revealed that the LUMO energy level of HTB-co-P3HT was lowest in toluene compared to the other solvents used to prepare the thin films, owing to the influence of the boiling point and polarity of the solvent. EIS traces revealed higher impedance for HTB over HTB-co-P3HT for all solvents indicating that HTB-co-P3HT is more conductive than HTB. The highest PCE, of 0.48%, for the device was achieved in chlorobenzene because of faster electron mobility as verified by EIS studies, with toluene, which proved the best solvent for the HTB and HTB-co-P3HT, at a distant second.

DATA AVAILABILITY STATEMENT

The original contributions presented in the study are included in the article/Supplementary Material, further inquiries can be directed to the corresponding authors.

AUTHOR CONTRIBUTIONS

MR writing-original draft, methodology, formal analysis, investigation, SM, KJ, SY, KN, and KVM methodology and data curation. VJ-D and KDM supervision, writing, reviewing and editing. AW writing, reviewing and editing. EI project conceptualization and experimental design, supervision and editing. All authors have read and approved the manuscript for publication.

FUNDING

REFERENCES

Afraj, S. N., He, G. Y., Lin, C. Y., Velusamy, A., Huang, C. Y., Lin, P. S., et al. (2021). Solution-Processable Multifused Thiophene Small Molecules and Conjugated Polymer Semiconducting Blend for Organic Field Effect Transistor Application. *Adv. Mater. Technol.* 6 (3), 2001028. doi:10.1002/admt.202001028

Agrawal, V., Jain, K., Arora, L., and Chand, S. (2013). Synthesis of CdS Nanocrystals in Poly(3-Hexylthiophene) Polymer Matrix: Optical and Structural Studies. *J. Nanopart. Res.* 15 (6), 1–14. doi:10.1007/s11051-013-1697-z

Ansari, M. A., Mohiuddin, S., Kandemirli, F., and Malik, M. I. (2018). Synthesis and Characterization of Poly(3-Hexylthiophene): Improvement of Regioregularity and Energy Band Gap. *RSC Adv.* 8 (15), 8319–8328. doi:10.1039/c8ra00555a

Bahceci, S., and Esat, B. (2013). A Polyacetylene Derivative with Pendant TEMPO Group as Cathode Material for Rechargeable Batteries. *J. Power Sourc.* 242, 33–40. doi:10.1016/j.jpowsour.2013.05.051

Birnie, D. P., III (2013). A Model for Drying Control Cosolvent Selection for Spin-Coating Uniformity: The Thin Film Limit. *Langmuir* 29 (29), 9072–9078. doi:10.1021/la401106z

Boeva, Z. A., and Sergeyev, V. G. (2014). Polyaniline: Synthesis, Properties, and Application. *Polym. Sci. Ser. C* 56 (1), 144–153. doi:10.1134/S1811238214010032

Campos, J. F., and Berteina-Raboin, S. (2020). Eucalyptol as Bio-Based Solvent for Migita-Kosugi-Stille Coupling Reaction on O,S,N-Heterocycle. *Catal. Today* 358, 138–142. doi:10.1016/j.cattod.2019.11.004

Chan, D. H., Millet, A., Fisher, C. R., Price, M. C., Burchell, M. J., and Armes, S. P. (2021). Synthesis and Characterization of Polypyrrole-Coated Anthracene Microparticles: A New Synthetic Mimic for Polyaromatic Hydrocarbon-Based Cosmic Dust. *ACS Appl. Mater. Inter.* 13 (2), 3175–3185. doi:10.1021/acsami.0c19758

Chang, S. H., Chiang, C.-H., Cheng, H.-M., Tai, C.-Y., and Wu, C.-G. (2013). Broadband Charge Transfer Dynamics in P3HT:PCBM Blended Film. *Opt. Lett.* 38 (24), 5342–5345. doi:10.1364/ol.38.005342

Chen, F., Liu, Y., Pan, J., Zhu, A., Bao, J., Yue, X., et al. (2020). Carbazole-Modified Polyphenylene Ether as Host Materials for High Efficiency Phosphorescent Organic Light-Emitting Diodes. *Opt. Mater.* 101, 109781. doi:10.1016/j.optmat.2020.109781

Cui, B.-B., Han, Y., Yang, N., Yang, S., Zhang, L., Wang, Y., et al. (2018). Propeller-Shaped, Triarylamine-Rich, and Dopant-Free Hole-Transporting Materials for Efficient N-I-P Perovskite Solar Cells. *ACS Appl. Mater. Inter.* 10 (48), 41592–41598. doi:10.1021/acsami.8b15423

Cui, C., and Wong, W.-Y. (2016). Effects of Alkylthio and Alkoxy Side Chains in Polymer Donor Materials for Organic Solar Cells. *Macromol. Rapid Commun.* 37 (4), 287–302. doi:10.1002/marc.201500620

Cui, Y., Wu, Y., Lu, X., Zhang, X., Zhou, G., Miapeh, F. B., et al. (2011). Incorporating Benzotriazole Moiety to Construct D-A-π-A Organic Sensitizers for Solar Cells: Significant Enhancement of Open-Circuit Photovoltage with Long Alkyl Group. *Chem. Mater.* 23 (19), 4394–4401. doi:10.1021/cm202226j

Diantoro, M., Suprayogi, T., Hidayat, A., Taufiq, A., Fuad, A., and Suryana, R. (2018). Shockley's Equation Fit Analyses for Solar Cell Parameters from I-V Curves. *Int. J. Photoenergy* 2018, 1–7. doi:10.1155/2018/9214820

Dikcal, F., Topal, S., Unal, M., and Ozturk, T. (2020). Synthesis, Characterization and Electrochemical Properties of Polymers Based on Dithienothiophene and Bithiazole. *Asian J. Org. Chem.* 9 (9), 1309–1317. doi:10.1002/ajoc.202000213

Ekbote, A., Jadhav, T., and Misra, R. (2017). T-Shaped Donor-Acceptor-Donor Type Tetraphenylethylene Substituted Quinoxaline Derivatives: Aggregation-Induced Emission and Mechanochromism. *New J. Chem.* 41 (17), 9346–9353. doi:10.1039/c7nj01531c

El-Bashir, S. M. (2019). Effect of Solvent Polarity on the Homogeneity and Photophysical Properties of MDMO-PPV Films: Towards Efficient Plastic Solar Cells. *J. King Saud Univ. - Sci.* 31 (4), 534–540. doi:10.1016/j.jksus.2017.09.008

Fan, Q., Ma, R., Liu, T., Yu, J., Xiao, Y., Su, W., et al. (2021). High-Performance All-Polymer Solar Cells Enabled by a Novel Low Bandgap Non-Fully Conjugated Polymer Acceptor. *Sci. China Chem.* 64, 1380–1388. doi:10.1007/s11426-021-1020-7

Fei, Z., Boufflet, P., Wood, S., Wade, J., Moriarty, J., Gann, E., et al. (2015). Influence of Backbone Fluorination in Regioregular Poly(3-Alkyl-4-Fluoro) thiophenes. *J. Am. Chem. Soc.* 137 (21), 6866–6879. doi:10.1021/jacs.5b02785

Gao, K., Kan, Y., Chen, X., Liu, F., Kan, B., Nian, L., et al. (2020). Low-Bandgap Porphyrins for Highly Efficient Organic Solar Cells: Materials, Morphology, and Applications. *Adv. Mater.* 32 (32), 1906129. doi:10.1002/adma.201906129

Gautam, P., Sharma, R., Misra, R., Keshtov, M. L., Kuklin, S. A., and Sharma, G. D. (2017). Donor-Acceptor-Acceptor (D-A-A) Type 1,8-naphthalimides as Non-Fullerene Small Molecule Acceptors for Bulk Heterojunction Solar Cells. *Chem. Sci.* 8 (3), 2017–2024. doi:10.1039/c6sc04461a

Gholizadeh, A., Reyhani, A., Parvin, P., and Mortazavi, S. Z. (2017). Efficiency Enhancement of ZnO Nanostructure Assisted Si Solar Cell Based on Fill Factor Enlargement and UV-Blue Spectral Down-Shifting. *J. Phys. D: Appl. Phys.* 50 (18), 185501. Available at: http://iopscience.iop.org/0022-3727/50/18/185501. doi:10.1088/1361-6463/aa6454

Gupta, S., Sharma, A., and Verma, R. S. (2020). Polymers in Biosensor Devices for Cardiovascular Applications. *Curr. Opin. Biomed. Eng.* 13, 69–75. doi:10.1016/j.cobme.2019.10.002

Hu, Z., Willard, A. P., Ono, R. J., Bielawski, C. W., Rossky, P. J., and Vanden Bout, D. A. (2015). An Insight into Non-Emissive Excited States in Conjugated Polymers. *Nat. Commun.* 6 (1), 1–9. doi:10.1038/ncomms9246

Huang, J.-H., Ibrahem, M. A., and Chu, C.-W. (2013). Interfacial Engineering Affects the Photocatalytic Activity of Poly (3-Hexylthiophene)-Modified TiO₂. *RSC Adv.* 3 (48), 26438–26442. doi:10.1039/C3RA43393E

Jeong, C., Nagai, T., Ishizuka, S., Tampo, H., Hajime, S., Kim, S., et al. (2021). Examination of Suitable Bandgap Grading of Cu(InGa)Se₂ Bottom Absorber Layers for Tandem Cell Application. *Phys. Status Solidi A.* 218 (10), 2000658. doi:10.1002/pssa.202000658

Joseyphus, R. S., and Nair, M. S. (2010). Synthesis, Characterization and Biological Studies of Some Co (II), Ni (II) and Cu (II) Complexes Derived from Indole-3-Carboxaldehyde and Glycylglycine as Schiff Base Ligand. *Arab. J. Chem.* 3 (4), 195–204. doi:10.1016/j.arabjc.2010.05.001

Kettle, J., Ding, Z., Horie, M., and Smith, G. C. (2016). XPS Analysis of the Chemical Degradation of PTB7 Polymers for Organic Photovoltaics. *Org. Electron.* 39, 222–228. doi:10.1016/j.orgel.2016.10.016

Khalaji, A., and Das, D. (2015). Preparation of CuO Nanoparticles by Thermal Decomposition of Double-Helical Dinuclear Copper (II) Schiff-Base Complexes. *J. Ultrafine Grained Nanostruct. Mater.* 48 (2), 93–99. doi:10.7508/jufgnsm.2015.02.004

Khokhar, D., Jadoun, S., Arif, R., and Jabin, S. (2021). Functionalization of Conducting Polymers and Their Applications in Optoelectronics. *Polymer-Plastics Technol. Mater.* 60 (5), 465–487. doi:10.1080/25740881.2020.1819312

Kim, J., Duraisamy, N., Lee, T.-M., Kim, I., and Choi, K.-H. (2015). Screen Printed Silver Top Electrode for Efficient Inverted Organic Solar Cells. *Mater. Res. Bull.* 70, 412–415. doi:10.1016/j.materresbull.2015.04.052

Kim, J. (2019). Effect of Solvents on the Electrical and Morphological Characteristics of Polymer Solar Cells. *Polymers* 11 (2), 228. doi:10.3390/polym11020228

Kim, Y., Cook, S., Kirkpatrick, J., Nelson, J., Durrant, J. R., Bradley, D. D. C., et al. (2007). Effect of the End Group of Regioregular Poly(3-Hexylthiophene) Polymers on the Performance of Polymer/Fullerene Solar Cells. *J. Phys. Chem. C* 111 (23), 8137–8141. doi:10.1021/jp072306z

Le, T.-H., Kim, Y., and Yoon, H. (2017). Electrical and Electrochemical Properties of Conducting Polymers. *Polymers* 9 (4), 150. doi:10.3390/polym9040150

Leitner, T. D., Gmeinder, Y., Röhricht, F., Herges, R., Mena-Osteritz, E., and Bäuerle, P. (2020). Twisted Thienylene-Phenylene Structures: Through-Space Orbital Coupling in Toroidal and Catenated Topologies. *Eur. J. Org. Chem.* 2020 (3), 285–294. doi:10.1002/ejoc.201901637

Liu, F., Nguyen, T.-P., Wang, Q., Massuyeau, F., Dan, Y., and Jiang, L. (2019). Construction of Z-Scheme G-C₃N₄/Ag/P3HT Heterojunction for Enhanced Visible-Light Photocatalytic Degradation of Tetracycline (TC) and Methyl orange (MO). *Appl. Surf. Sci.* 496, 143653. doi:10.1016/j.apsusc.2019.143653

Liu, X., Liang, Z., Du, S., Tong, J., Li, J., Zhang, R., et al. (2021). Non-Halogenated Polymer Donor-Based Organic Solar Cells with a Nearly 15% Efficiency Enabled by a Classic Ternary Strategy. *ACS Appl. Energ. Mater.* 4 (2), 1774–1783. doi:10.1021/acsaem.0c02912

Liu, X., Zheng, Z., Xu, Y., Wang, J., Wang, Y., Zhang, S., et al. (2020). Quantifying Voc Loss Induced by Alkyl Pendants of Acceptors in Organic Solar Cells. *J. Mater. Chem. C* 8 (36), 12568–12577. doi:10.1039/d0tc01941k

Mei, B.-A., Lau, J., Lin, T., Tolbert, S. H., Dunn, B. S., and Pilon, L. (2018). Physical Interpretations of Electrochemical Impedance Spectroscopy of Redox Active Electrodes for Electrical Energy Storage. *J. Phys. Chem. C* 122 (43), 24499–24511. doi:10.1021/acs.jpcc.8b05241

Mota, I. C., Santos, B. P. S., dos Santos, R. É. P., Guedes, L. B., Soares, I. T., Arias, J. J. R., et al. (2021). Influence of Reaction Time on Properties of Regioregular Poly(3-Hexylthiophene) by the Grignard Metathesis Polymerization. *J. Therm. Anal. Calorim.* 147, 5037–5048. doi:10.1007/s10973-021-10890-4

Naureen, B., Miana, G. A., Shahid, K., Asghar, M., Tanveer, S., and Sarwar, A. (2021). Iron (III) and Zinc (II) Monodentate Schiff Base Metal Complexes: Synthesis, Characterisation and Biological Activities. *J. Mol. Struct.* 1231, 129946. doi:10.1016/j.molstruc.2021.129946

Nayana, V., and Kandasubramanian, B. (2020). Polycarbazole and its Derivatives: Progress, Synthesis, and Applications. *J. Polym. Res.* 27 (9), 1–24. doi:10.1007/s10965-020-02254-7

Niefind, F., Karande, S., Frost, F., Abel, B., and Kahnt, A. (2019). Solvent Influence on the Surface Morphology of P3HT Thin Films Revealed by Photoemission Electron Microscopy. *Nanoscale Adv.* 1 (10), 3883–3886. doi:10.1039/c9na00419j

Park, J., Moon, H. C., and Kim, J. K. (2013). Facile Synthesis for Well-Defined A2B Miktoarm star Copolymer of Poly(3-Hexylthiophene) and Poly(methyl Methacrylate) by the Combination of Anionic Polymerization and Click Reaction. *J. Polym. Sci. A. Polym. Chem.* 51 (10), 2225–2232. doi:10.1002/pola.26604

Pei, J., Hao, Y. Z., Lv, H. J., Sun, B., Li, Y. P., and Guo, Z. M. (2016). Optimizing the Performance of TiO₂/P3HT Hybrid Solar Cell by Effective Interfacial Modification. *Chem. Phys. Lett.* 644, 127–131. doi:10.1016/j.cplett.2015.11.058

Pei, L. Z., Ma, Y., Qiu, F. L., Lin, F. F., Fan, C. G., and Ling, X. Z. (2019). In-Ssitu Synthesis of Polynaphthylamine/Graphene Composites for the Electrochemical Sensing of Benzoic Acid. *Mater. Res. Express* 6 (1), 015053. doi:10.1088/2053-1591/aae96e

Rafique, S., Abdullah, S. M., Badiei, N., McGettrick, J., Lai, K. T., Roslan, N. A., et al. (2020). An Insight into the Air Stability of the Benchmark Polymer:Fullerene Photovoltaic Films and Devices: A Comparative Study. *Org. Electron.* 76, 105456. doi:10.1016/j.orgel.2019.105456

Rahman, M. H., Liao, S.-C., Chen, H.-L., Chen, J.-H., Ivanov, V. A., Chu, P. P. J., et al. (2009). Aggregation of Conjugated Polymers in Aromatic Solvent. *Langmuir* 25 (3), 1667–1674. doi:10.1021/la802526d

Ramoroka, M. E., Mdluli, S. B., John-Denk, V. S., Modibane, K. D., Arendse, C. J., and Iwuoha, E. I. (2021). Synthesis and Photovoltaics of Novel 2,3,4,5-Tetrathienylthiophene-Co-Poly(3-Hexylthiophene-2,5-Diyl) Donor Polymer for Organic Solar Cell. *Polymers* 13 (1), 2. doi:10.3390/polym13010002

Rasmussen, S. C. (2015). Early History of Polypyrrole: the First Conducting Organic Polymer. *Bull. Hist. Chem.* 40 (1), 45–55.

Salaiman, N. M., Taura, L. S., Lawal, A., Gidado, A. S., and Musa, A. (2019). Solvent Effects on the Structural, Electronic, Non-linear Optical and Thermodynamic Properties of Perylene Based on Density Functional Theory. *J. Mater. Sci. Res. Rev.* 3 (3), 1–13.

Sancho, M. I., Almandoz, M. C., Blanco, S. E., and Castro, E. A. (2011). Spectroscopic Study of Solvent Effects on the Electronic Absorption Spectra

of Flavone and 7-hydroxyflavone in Neat and Binary Solvent Mixtures. *Int. J. Mol. Sci.* 12 (12), 8895–8912. doi:10.3390/ijms12128895

Shi, C., Yao, Y., Yang, Y., and Pei, Q. (2006). Regioregular Copolymers of 3-alkoxythiophene and Their Photovoltaic Application. *J. Am. Chem. Soc.* 128 (27), 8980–8986. doi:10.1021/ja061664x

Tamanai, A., Beck, S., and Pucci, A. (2013). Mid-Infrared Characterization of Thiophene-Based Thin Polymer Films. *Displays* 34 (5), 399–405. doi:10.1016/j.displa.2013.08.005

Tanaka, S., Rosli, S. K. B., Takada, K., Taniai, N., Yoshitomi, T., Ando, H., et al. (2017). Effects of Bromination of Poly(3-Hexylthiophene) on the Performance of Bulk Heterojunction Solar Cells. *RSC Adv.* 7 (74), 46874–46880. doi:10.1039/c7ra07454a

Tang, A., Li, J., Zhang, B., Peng, J., and Zhou, E. (2020). Low-Bandgap N-Type Polymer Based on a Fused-DAD-Type Heptacyclic Ring for All-Polymer Solar Cell Application with a Power Conversion Efficiency of 10.7%. *ACS Macro Lett.* 9 (5), 706–712. doi:10.1021/acsmacrolett.0c00234

Valderrama-García, B., Rodríguez-Alba, E., Morales-Espinoza, E., Moineau Chane-Ching, K., and Rivera, E. (2016). Synthesis and Characterization of Novel Polythiophenes Containing Pyrene Chromophores: thermal, Optical and Electrochemical Properties. *Molecules* 21 (2), 172. doi:10.3390/molecules21020172

Wang, D. H., Kim, J. K., Seo, J. H., Park, O. O., and Park, J. H. (2012). Stability Comparison: A PCDTBT/PC$_{71}$BM Bulk-Heterojunction Versus a P3HT/PC$_{71}$BM Bulk-Heterojunction. *Sol. Energ. Mater. Sol. Cell* 101, 249–255. doi:10.1016/j.solmat.2012.02.005

Wang, Z., Zhu, M., Pei, Z., Xue, Q., Li, H., Huang, Y., et al. (2020). Polymers for Supercapacitors: Boosting the Development of the Flexible and Wearable Energy Storage. *Mater. Sci. Eng. R: Rep.* 139, 100520. doi:10.1016/j.mser.2019.100520

Warad, I., Ali, O., Al Ali, A., Jaradat, N. A., Hussein, F., Abdallah, L., et al. (2020). Synthesis and Spectral Identification of Three Schiff Bases with a 2-(Piperazin-1-yl)-N-(thiophen-2-yl Methylene)ethanamine Moiety Acting as Novel Pancreatic Lipase Inhibitors: Thermal, DFT, Antioxidant, Antibacterial, and Molecular Docking Investigations. *Molecules* 25 (9), 2253. doi:10.3390/molecules25092253

Xiao, L., Mao, H., Li, Z., Yan, C., Liu, J., Liu, Y., et al. (2020). Employing a Narrow-Band-Gap Mediator in Ternary Solar Cells for Enhanced Photovoltaic Performance. *ACS Appl. Mater. Inter.* 12 (14), 16387–16393. doi:10.1021/acsami.9b23516

Yadav, P. K., Prakash, O., Ray, B., and Maiti, P. (2021). Functionalized Polythiophene for Corrosion Inhibition and Photovoltaic Application. *J. Appl. Polym. Sci.* 138, 51306. doi:10.1002/app.51306

Ye, D., Li, X., Yan, L., Zhang, W., Hu, Z., Liang, Y., et al. (2013). Dithienosilole-Bridged Small Molecules with Different Alkyl Group Substituents for Organic Solar Cells Exhibiting High Open-Circuit Voltage. *J. Mater. Chem. A.* 1 (26), 7622–7629. doi:10.1039/c3ta11257h

Yoshida, K., Morimoto, I., Mitsudo, K., and Tanaka, H. (2008a). Facile Synthetic Procedure for and Electrochemical Properties of Hexa(2-Thienyl)benzenes Directed toward Electroactive Materials. *Tetrahedron Lett.* 49 (15), 2363–2365. doi:10.1016/j.tetlet.2008.02.069

Yoshida, K., Morimoto, I., Mitsudo, K., and Tanaka, H. (2008b). RhCl$_3$/amine-Catalyzed [2+ 2+ 2] Cyclization of Alkynes. *Tetrahedron* 64 (24), 5800–5807. doi:10.1016/j.tet.2008.03.079

Zhang, S., Qin, Y., Zhu, J., and Hou, J. (2018). Over 14% Efficiency in Polymer Solar Cells Enabled by a Chlorinated Polymer Donor. *Adv. Mater.* 30 (20), 1800868. doi:10.1002/adma.201800868

Zhang, Y., Gao, X., Li, J., and Tu, G. (2015). Highly Selective Palladium-Catalyzed Suzuki Coupling Reaction toward Chlorine-Containing Electroluminescence Polymers. *Dyes Pigm.* 120, 112–117. doi:10.1016/j.dyepig.2015.03.031

Zhang, Z., Liang, L., Deng, L., Ren, L., Zhao, N., Huang, J., et al. (2021). Fused Dithienopicenocarbazole Enabling High Mobility Dopant-Free Hole-Transporting Polymers for Efficient and Stable Perovskite Solar Cells. *ACS Appl. Mater. Inter.* 13 (5), 6688–6698. doi:10.1021/acsami.0c21729

Zhao, H., Wang, Z., Dong, G., and Duan, L. (2015). Fabrication of Highly Oriented Large-Scale TIPS Pentacene Crystals and Transistors by the Marangoni Effect-Controlled Growth Method. *Phys. Chem. Chem. Phys.* 17 (9), 6274–6279. doi:10.1039/c4cp05378h

Zheng, B., Qi, F., Zhang, Y., Zhang, M., Gao, P., Liu, F., et al. (2021). Over 14% Efficiency Single-Junction Organic Solar Cells Enabled by Reasonable Conformation Modulating in Naphtho [2, 3-b: 6, 7-b'] Difuran Based Polymer. *Adv. Ener. Mater.* 11 (13), 2003954. doi:10.1002/aenm.202003954

Zhou, H., Yang, L., and You, W. (2012). Rational Design of High Performance Conjugated Polymers for Organic Solar Cells. *Macromolecules* 45 (2), 607–632. doi:10.1021/ma201648t